PCCP

PAPER

View Article Online
View Journal | View Issue

Cite this: *Phys. Chem. Chem. Phys.*, 2025, **27**, 2680

Pressure-dependent kinetic analysis of the N_2H_3 potential energy surface†

Michal Keslin,[a] Kfir Kaplan[a] and Alon Grinberg Dana *[ab]

Received 5th October 2024,
Accepted 6th January 2025

DOI: 10.1039/d4cp03837a

rsc.li/pccp

The pressure-dependent reactions on the N_2H_3 potential energy surface (PES) have been investigated using CCSD(T)-F12/aug-cc-pVTZ-F12//B2PLYP-D3/aug-cc-pVTZ. This study expands the N_2H_3 PES beyond the previous literature by incorporating a newly identified isomer, NH_3N, along with additional bimolecular reaction channels associated with this isomer, namely NNH + H_2 and $H_2NN(S)$ + H. Rate coefficients for all relevant pressure-dependent reactions, including well-skipping pathways, are predicted using a combination of *ab initio* transition state theory and master equation simulations. The dominant product of the NH_2 + NH(T) recombination is N_2H_2 + H, while at high pressures and low temperatures, N_2H_3 formation becomes significant. Similarly, collisions involving $H_2NN(S)$ + H predominantly produce N_2H_2 + H. Secondary reactions such as $H_2NN(S)$ + H ⇌ NNH + H_2 and $H_2NN(S)$ + H ⇌ NH_2 + NH(T) are found to play a significant role at high temperatures across all examined pressures, while $H_2NN(S)$ + H ⇌ NH_3N becomes prominent only at high pressures. Notably, none of these four $H_2NN(S)$ reactions have been included with pressure-dependent rate coefficients in previous NH_3 oxidation models. The rate coefficients reported here provide valuable insights for modeling the combustion of ammonia, hydrazine, and their derivatives in diverse environments.

1. Introduction

Nitrogen-based fuels, including ammonia (NH_3),[1] hydrazine (N_2H_4),[2,3] hydrazine derivatives such as monomethylhydrazine (MMH, CH_3NHNH_2),[2] and aqueous formulations,[4,5] form a versatile class of energy carriers. Hydrazine and its derivatives are widely used as satellite and spacecraft propellants, while ammonia receives an increasing interest as a potential energy storage vector.[6] In the envisioned future nitrogen economy,[7] ammonia is expected to play a key role. Despite differences in their specific applications, the chemical kinetic modeling of these nitrogen-based fuels relies on a shared core chemistry and a set of fundamental reactions.[8]

Hydrazine, a principal component of diamine-based rocket propellants, stands out as an efficient mono- and bi-propellant. Paired with oxygen as an oxidizer, it is second only to hydrogen in terms of specific impulse—the thrust generated per unit mass of fuel over time.[3] Hydrazine can be used as a monopropellant, typically undergoing decomposition using a catalyst,[3] leading to autoignition and detonation.[9–11] Furthermore, hydrazine and hydrazine-based fuels, including MMH, function as bipropellants when combined with nitrogen tetroxide (N_2O_4) as the oxidizer. These fuels are ubiquitous as thruster engine propellants for satellite and spacecraft attitude control and in-orbit maneuvers,[3] where they are stored and used at a maximum pressure of ~25 bar.[12–14]

Nitrogen-based alternative fuels are particularly attractive due to the abundance of molecular atmospheric nitrogen as a feedstock. Among them, ammonia is the simplest molecule and it shows significant promise as an energy storage vector.[1,6,15] The advantages of ammonia as a fuel include a relatively high power-to-fuel-to-power (PFP) efficiency,[7] a large-scale distribution infrastructure that is already in place,[16,17] a high octane rating,[18] and a narrow flammability range that makes it relatively safe in terms of explosion risks. Although kinetic modeling of NH_3 oxidation received significant attention lately,[19–35] there is still substantial disagreements on thermodynamic data and rate coefficients between different authors in this relatively small chemical system.[8,36–39]

[a] *Wolfson Department of Chemical Engineering, Technion – Israel Institute of Technology, Haifa 3200003, Israel. E-mail: alon@technion.ac.il; Tel: +972-73-378-2117*
[b] *Grand Technion Energy Program (GTEP), Technion – Israel Institute of Technology, Haifa 3200003, Israel*

† Electronic supplementary information (ESI) available: Stationary points geometries, T1 diagnostic factors, and imaginary frequencies (Table S1). Torsional scan of N_2H_3 at a resolution of 10° at the B2PLYP-D3/aug-cc-pVTZ level (Fig. S1). Representation of the N_2H_3 PES along with energy values from previous studies (Fig. S2). NH_3N Thermodynamic properties, Chemkin format (Table S2). NH_3N Thermodynamic properties, Cantera format (Table S3). Computed rate coefficient, Chemkin format (Table S4). Computed rate coefficient, Cantera format (Table S5). 3D representations of species (Fig. S3–S7). Species internal coordinate comparisons (Tables S6–S10). An unsuccessful TS search for the N_2H_3 ⇌ H2NN(S) + H reaction (Fig. S8). A scan of the N– –H distance in the N_2H_3 ⇌ $H_2NN(S)$ + H reaction (Fig. S9). Estimated reaction rate uncertainty based on computed energies (Fig. S10). Comparison of experimental and computed frequencies (Table S11). See DOI: https://doi.org/10.1039/d4cp03837a

Konnov and De Ruyck[40] suggested a chemical kinetic model for hydrazine decomposition, and Izato *et al.*[41] suggested a model for the initial hypergolic reaction of liquid hydrazine with nitrogen tetroxide mixtures. Hydrazine decomposition was also studied by Asatryan *et al.*,[42] and its key pathways in hypergolic ignition with nitrogen dioxide and nitrogen tetroxide were suggested by Raghunath *et al.*[43] and by Daimon *et al.*,[44] respectively. The thermal decomposition of hydrazine was studied using a reactive force field.[45] Hydrazine decomposition on catalytic surfaces was also studied theoretically.[46,47] Sun and Law[48] developed a model for thermal decomposition of MMH, and Zhang *et al.*[49] performed a theoretical analysis of the kinetics of barrierless recombination reactions in the MMH system as well as secondary channels.[50] Although chemical kinetic models were previously suggested to predict the reactivity of hydrazine and its derivative, the research on the combustion of these fuels has been based on incomplete kinetic mechanisms, which may not fully capture all the relevant reaction pathways. Despite the development of detailed kinetic models, there is a demand for more advanced modeling approaches.[51]

The present work focuses on studying the N_2H_3 potential energy surface (PES) that is relevant for all the chemical systems mentioned above. This PES was previously studied by Klippenstein *et al.*[52] at the CCSD(T)/CBS//CCSD(T)/aug-cc-pVDZ level of theory when exploring reactions originating from the NH_2 + NH channel. Klippenstein *et al.* showed that the reaction proceeds through the abstraction of an H atom on the quartet surface (forming NH_3 + N(Q)) or by addition followed by H atom elimination on the doublet surface (forming N_2H_2 + H), as shown in Fig. 1(A). They computed a rate coefficient for the barrierless initial addition of NH_2 + NH(T) using variable reaction-coordinate transition state theory (VRC-TST). The authors stated that a transition state (TS) is likely to exist for H_2 elimination from N_2H_3 but was not found in the cited study.[52] They expected such a TS to lie higher in energy than that for H loss, and thus it should make an insignificant contribution to the kinetics. Raghunath *et al.*[43] slightly refined the pressure-dependent network by explicitly considering the *cis* and *trans* isomers of N_2H_2, but did not consider the barrierless addition reaction (Fig. 1(B)). Diévart and Catoire[53] used the high-pressure VRC-TST rate coefficient calculated by Klippenstein *et al.*[52] along with an inverse Laplace transform (ILT)[54] to suggest pressure-dependent reaction rate coefficients for reactions $N_2H_3 + M \rightleftharpoons NH_2 + NH + M$ and $N_2H_3 + M \rightleftharpoons N_2H_2 + H$. However, they also only considered the *trans* isomer of the N_2H_2 product (Fig. 1(C)) and did not provide a rate coefficient for the well-skipping reaction $NH_2 + NH(T) \rightleftharpoons N_2H_2 + H$.

Pressure-dependent rate coefficients have not previously been reported for the $NH_2 + NH(T) \rightleftharpoons N_2H_2 + H$ and $N_2H_2 + H \rightleftharpoons NNH + H_2$ reactions, nor for any reaction on this PES involving the $H_2NN(S) + H$ well, such as the formation of $N_2H_2 + H$, $NNH + H_2$, or N_2H_3. Currently, the literature lacks a comprehensive description of the N_2H_3 PES, as well as a complete set of pressure-dependent reaction rate coefficients for all relevant pathways. The goal of the present work is to address these gaps and provide kinetic modellers of nitrogen-based fuel systems with high-quality kinetic data for the unimolecular N_2H_3 system.

2. Methods

Ab initio calculations were carried out using the open source Automated Rate Calculator (ARC) software suite,[55] which automates the calculation of species thermochemistry and reaction rate coefficients. Conformer geometry searches were performed based on a random set of force field conformers generated *via* RDKit[56] using MMFF94s.[57] The force field conformers were optimized at the ωB97X-D/Def2-SVP[58,59] level of theory. The lowest energy DFT (density functional theory) conformer was further used and optimized at the double-hybrid B2PLYP functional[60] with Grimme's dispersion correction, D3(BJ),[61] coupled with Dunning's correlation consistent basis set[62] augmented with diffuse functions, *i.e.*, B2PLYP-D3/aug-cc-pVTZ. Ro-vibrational analyses were subsequently computed *via* ARC at the same level of theory. ARC calculated a frequency scaling

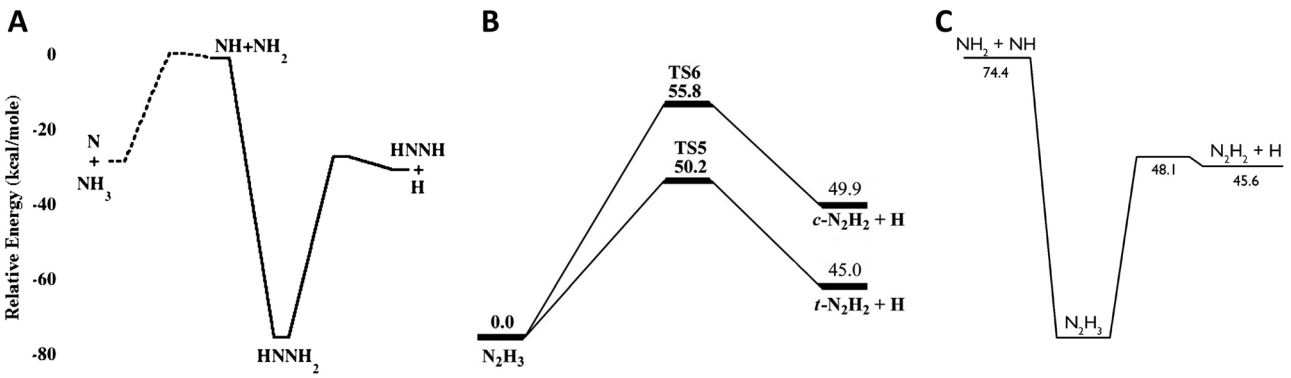

Fig. 1 Representations of the N_2H_3 PES from previous literature works in kcal mol^{-1}. (A) CCSD(T)/CBS//CCSD(T)/aug-cc-pVDZ level of theory calculations by Klippenstein *et al.*[52] The solid and dashed lines correspond to the doublet and quartet surfaces, respectively. (B) CCSD(T)/CBS//MP2/6-311++G(3df,2p) level of theory calculations by Raghunath *et al.*[43] on the doublet surface (this inset is not plotted to scale, as in the original manuscript). (C) RCCSD(T)/CBS//M06-2x-D3/aug-cc-pVTZ level of theory calculation by Diévart and Catoire[53] on the doublet surface. Usage rights: (A) Reprinted (adapted) with permission from *J. Phys. Chem. A* 2009, **113**, 38, 10241–10259. Copyright 2009 American Chemical Society. (B) Reprinted from Publication P. Raghunath, N. T. Nghia, M.-C. Lin "Chapter Seven – *Ab Initio* Chemical Kinetics of Key Processes in the Hypergolic Ignition of Hydrazine and Nitrogen Tetroxide", *Adv. Quantum Chem.* **69**, 2014, 253–301, Copyright (2014), with permission from Elsevier. (C) Reprinted (adapted) with permission from *J. Phys. Chem. A* 2020, **124**, 30, 6214–6236. Copyright 2020 American Chemical Society.

factor of 0.995 for this functional and basis set combination using the method recommended by Truhlar *et al.*[63] Quantum tunneling effects were incorporated using the Eckart correction.[64] TS verification was performed by intrinsic reaction coordinate (IRC) computations[65] and automated inspection of the normal mode displacement.

Torsional modes were automatically identified as rotatable single bonds (accounting for relevant resonance structures[66]) and treated with continuous constrained optimizations with all other internal coordinates relaxed using the B2PLYP-D3/aug-cc-pVTZ level of theory at a dihedral angle resolution of 10°. The 1D potential energy torsional scans were fitted to truncated Fourier series that were used as input to compute energy levels and the partition function of anharmonic modes using Arkane,[67] an open source software distributed within the RMG software suite.[68] All DFT calculations were performed in Gaussian 09.[69]

Single-point energies were computed using three methods: 1. CCSD(T)-F12[70–72] with the correlation-consistent aug-cc-pVTZ-F12 base set,[62,73] 2. MRCI-F12+Q (internal contracted multiconfiguration reference configuration-interaction with explicit correlation F12 and Davidson correction)[74–76] with the same basis set, and 3. CCSDT(Q),[77] which approximates full CCSDTQ calculations[78] by extending coupled-cluster theory to include full triples excitations (CCSDT) with a perturbative treatment of connected quadruple excitations, using the aug-cc-pVTZ basis set. The MRCI-F12+Q calculations were performed with the full valence active space that included 13 valence electrons and 11 active orbitals for the isomers and TSs on the N_2H_3 PES. The CCSD(T)-F12 and MRCI-F12+Q calculations were performed in Molpro 2021.2,[79] and the CCSDT(Q) calculations were performed in Psi4 v. 1.9.1.[80] The frozen core approximation was applied to the CCSDT(Q) computations, wherein the 1s orbitals of nitrogen atoms were kept frozen while the valence and virtual orbitals were fully correlated. This approach effectively reduces computational cost without significantly compromising the accuracy of energy calculations. Empirical systematic errors in atomization energies were corrected using atom energy corrections implemented in Arkane[67,81] for the respective levels of theory.

Statistical mechanics processing of all electronic structure calculations were done by Arkane[67] to calculate the thermochemical partition functions and macroscopic parameters, including reaction rate coefficients of interest. Pressure-dependent reaction networks were modeled using a master equation (ME) describing molecular processes on a collisional timescale.[82] The Modified Strong Collision (MSC) approximation[83] was used to solve the ME since the more accurate Chemically Significant Eigenvalues (CSE) method[84] did not converge for this case. Collision energy transfer rates for deactivating collisions were modeled using the ''single exponential down'' expression, $\langle \Delta E_d \rangle$, with nitrogen as the bath gas. Nitrogen-based systems exhibit a somewhat different trend of $\langle \Delta E_d \rangle$ *vs.* temperature than carbon-based systems.[67] Since both $N_4H_6 + N_2$ and $N_3H_5 + N_2$ were shown to have relatively similar values,[67] the parameters computed for the $N_3H_5 + N_2$ system are assumed to be representative of the present $N_2H_3 + N_2$ system as well, and were adopted here: $\langle \Delta E_d \rangle = 175 \cdot (T/298\ \mathrm{K})^{0.52}\ \mathrm{cm}^{-1}$. Lennard-Jones parameters were taken from RMG's ''OneDMinN2'' transport library[85] computed using OneDMin,[86] and from Glarborg *et al.*[19]

An ILT,[54] a method of deriving microcanonical transition state theory rate coefficients as a function of the total energy from high-pressure limit rate coefficients, was used as implemented in Arkane[67] for the high-pressure limit recombination rate coefficient of the entrance channel NH_2 + NH(T) as determined by Klippenstein *et al.*,[52] and of the recombination channel $H_2NN(S)$ + H as estimated by RMG.[85] Pressure-dependent rate coefficients were fitted to Chebyshev polynomials[87] over a temperature range of 300–3000 K and a pressure range of 0.01–100 bar. Pressure-dependent network sensitivity analysis was performed using Arkane[67] by perturbing the *E*0 values of each well and TS in the PES and determining the effect on the calculated pressure-dependent rate coefficients.

3. Results and discussion

The doublet N_2H_3 PES (Fig. 2) involves pressure-dependent reactions among five bimolecular channels interconnected *via* two isomers, N_2H_3 and NH_3N (Fig. 3). Fig. S2 (ESI†) compares the present computations with the literature values shown in Fig. 1. The N_2H_3 radical is relatively stable, with an endothermic dissociation energy of ~200 kJ mol^{-1} (Fig. 2), significantly higher than similar beta-scission reactions.[88] The association of NH_2 + NH(T) (amino radical and triplet imidogen) without further isomerization can result in the formation of N_2H_3 or diazene (N_2H_2) and a hydrogen radical, as suggested by previous works.[43,52,53] However, the previous studies did not consider additional isomers in this PES other than N_2H_3 (Fig. 1). The NH_3N isomer (Fig. 2 and 3(B), SMILES[89] representation: [NH3+][N-]) is proposed as a conformation that facilitates further transformations on this PES. Thermodynamic properties for this isomer, calculated at the CCSD(T)-F12/cc-pVTZ-F12//B2PLYP-D3/aug-cc-pVTZ level of theory, are provided in Tables S2 and S3 (ESI†). The NH_3N isomer, a stable well in this PES, allows the pressure-dependent network to access two additional bimolecular wells: NNH + H_2 and $H_2NN(S)$ + H. The N_2H_3 isomer can also produce barrierlessly $H_2NN(S)$ + H (Fig. 2 and Fig. S8, S9, ESI†).

The NH_3 + N(D) bimolecular well, which is not shown in Fig. 2, was found to lie more than 400 kJ mol^{-1} above the N_2H_3 isomer (Table 1) and was therefore excluded from the ME analysis. This path originates from the NH_3N isomer. A TS for this channel was located using DFT, but its energy at the CCSDT(Q)/aug-cc-pVTZ level was lower than that of the corresponding bimolecular products. This reaction is likely barrierless, as previously determined for a similar reaction, CH_4 + N(D).[90] This channel is not important for the kinetics of N_2H_3 decomposition due to its high energy, although it might be relevant for plasma-assisted ammonia oxidation systems.[91]

Klippenstein *et al.*[52] commented that a TS which leads to the elimination of H_2 from N_2H_3 likely exists, but was not found in their study. Klippenstein *et al.* also noted that the missing TS is likely to have a higher energy than TSs for H loss and therefore this pathway should not contribute significantly to the

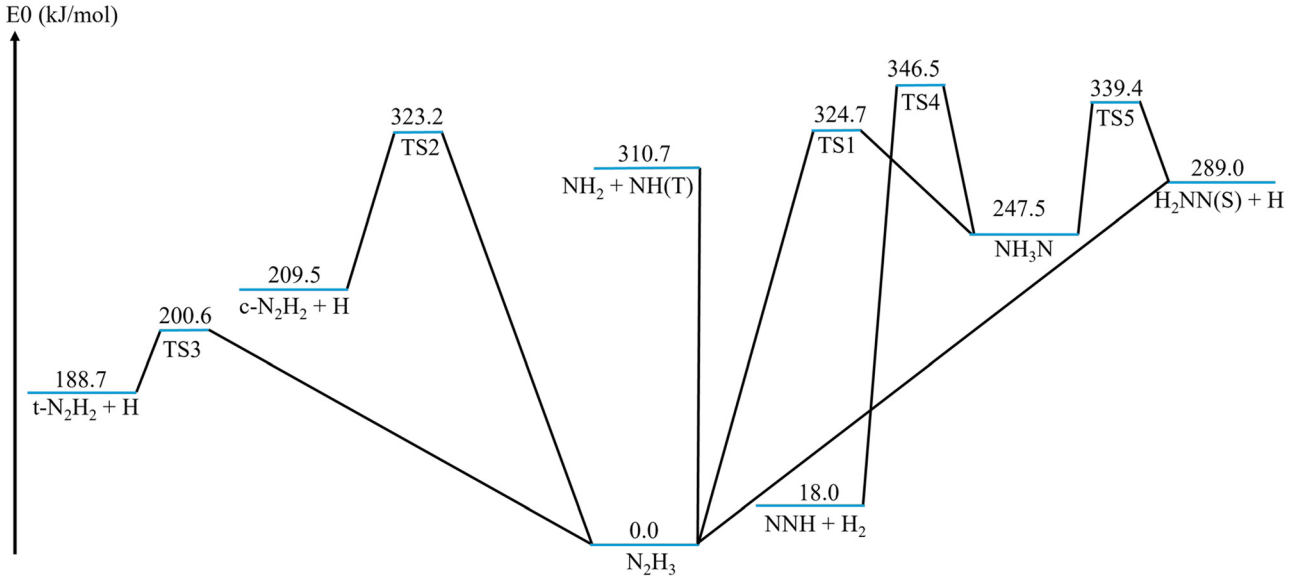

Fig. 2 The pressure-dependent kinetic network of the doublet N_2H_3 PES computed at the CCSD(T)-F12a/aug-cc-pVTZ-F12//B2PLYP-D3/aug-cc-pVTZ level of theory. Zero-point energies (electronic energy plus zero-point energy correction) are in kJ mol^{-1}.

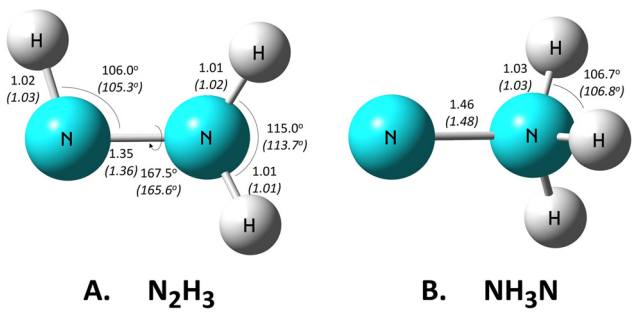

Fig. 3 Geometric representation of 3D structures of the two isomers on the explored PES, (A) N_2H_3 and (B) NH_3N, optimized at the B2PLYP-D3/aug-cc-pVTZ level of theory. Numbers represent internal coordinate values at the B2PLYP-D3/aug-cc-pVTZ level and in parenthesis at the CCSD/aug-cc-pVDZ level for comparison. The Cartesian coordinates are given in Table S1 (ESI†). Additional internal coordinate comparisons of computed geometries are given in Tables S6–S10 (ESI†).

kinetics.[52] In the present study, we were also unable to identify a TS corresponding to H_2 elimination directly from the N_2H_3 isomer. However, we show here that the elimination of H_2 in this PES stems from the NH_3N isomer (TS4, Fig. 2) rather than from N_2H_3. This TS was indeed found to lie significantly higher in energy than the H loss TSs (TS2 and TS3, Fig. 2). Consequently, this isomerization-mediated H_2 elimination channel from N_2H_3 or from NH_2 + NH(T) becomes relevant only at high temperature and low pressure conditions.

The NNH + H_2 products are the lowest-lying bimolecular well in this PES, whereas the *t*-N_2H_2 + H products' well is the most kinetically accessible from the NH_2 + NH(T) direction due to the relatively low energy barrier (TS3, Fig. 2). Another important entry channel into the N_2H_3 pressure-dependent system is the $H_2NN(S)$ + H well that could lead to either of the two isomers or to the NH_2 + NH(T), N_2H_2 + H, or NNH + H_2 bimolecular wells (Fig. 2).

Table 1 Description of stationary points (wells and TSs) on the N_2H_3 PES. Zero-point energy (*E*0) comparisons at CCSD(T)-F12a/aug-cc-pVTZ-F12, MRCI-F12+Q/aug-cc-pVTZ-F12, and CCSDT(Q)/aug-cc-pVTZ levels of theory are given in kJ mol^{-1} and are relative to the N_2H_3 isomer. Geometry optimization and frequency calculations for all methods were done at the B2PLYP-D3/aug-cc-pVTZ level of theory. Zero Kelvin enthalpy of formation values in kJ mol^{-1} are also given from the Active Thermochemical Tables (ATcT),[92] and are also relative to the N_2H_3 isomer

Stationary point	T1 diagnostic coefficient(s)	CCSD(T)-F12a	MRCI-F12+Q	CCSDT(Q)	ATcT
N_2H_3	0.025	0.0	0.0	0.0	0.0
NH_3N	0.012	247.5	234.6	243.9	—
NH_2 + NH(T)	0.008, 0.001	310.7	287.4	295.1	312.9
c-N_2H_2 + H	0.013, 0.000	209.5	194.9	196.3	210.1
t-N_2H_2 + H	0.013, 0.000	188.7	170.7	175.2	188.4
$H_2NN(S)$ + H	0.021, 0.000	289.0	270.6	276.5	288.8
NNH + H_2	0.028, 0.006	18.0	−2.4	16.5	17.4
NH_3 + N(D)	0.008, 0.006	447.4	413.8	415.3	427.2
TS1	0.025	324.7	311.6	324.7	
TS2	0.020	223.2	208.7	220.3	
TS3	0.021	200.6	190.5	197.3	
TS4	0.047	346.5	333.8	293.4	
TS5	0.088	339.4	321.6	321.9	

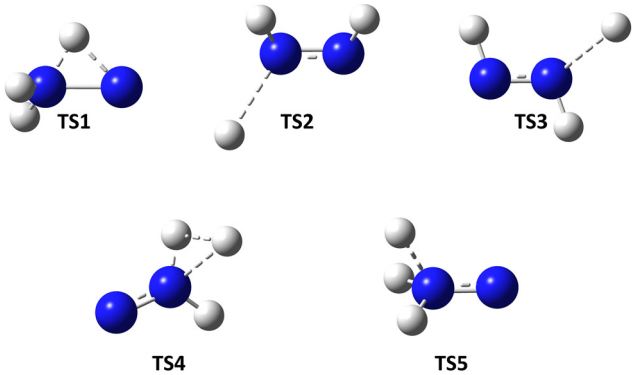

Fig. 4 Geometric representations of TSs on the N_2H_3 PES corresponding to the five non-barrierless path reactions, optimized at the B2PLYP-D3/aug-cc-pVTZ level of theory. Blue spheres represent nitrogen atoms, smaller light shaded balls represent hydrogen atoms, bond orders are given for illustration purposes only. Cartesian coordinates for all TS structures are available in Table S1 (ESI†).

Table 2 Deviations of $E0$ values computed at the different levels of theory relative to the N_2H_3 isomer from the corresponding ATcT values, units are kJ mol^{-1}

Stationary point	$\Delta E0$ CCSD(T)-F12a	$\Delta E0$ MRCI-F12+Q	$\Delta E0$ CCSDT(Q)
NH_2 + NH(T)	−2.20	−25.5	−17.80
c-N_2H_2 + H	−0.59	−15.20	−13.79
t-N_2H_2 + H	0.31	−17.70	−13.19
$H_2NN(S)$ + H	0.19	−18.21	−12.31
NNH + H_2	0.62	−19.78	−0.88

The geometries of the TSs identified in this PES are shown in Fig. 4. The computed imaginary frequencies of all TSs are provided in Table S1 (ESI†). Table 1 provides the T1 diagnostic coefficients[93–95] for all stationary points on the PES. It also lists the corresponding zero-point energies calculated at three levels of theory: CCSD(T)-F12a/aug-cc-pVTZ-F12, MRCI-F12+Q/aug-cc-pVTZ-F12, and CCSDT(Q)/aug-cc-pVTZ. All calculations were performed using B2PLYP-D3/aug-cc-pVTZ geometries and frequencies.

The energy deviations between the CCSD(T)-F12a and the CCSDT(Q) levels were approximately −9 kJ mol^{-1} on average, with a standard deviation of ∼15 kJ mol^{-1}. The energy deviations between the MRCI-F12+Q and the CCSDT(Q) levels averaged 6 kJ mol^{-1}, with a standard deviation of ∼15 kJ mol^{-1} as well (Table 1). All TSs in this PES, along with N_2H_3, NNH, and $H_2NN(S)$, have T1 diagnostic coefficients exceeding the 0.018–0.020 range, suggesting that a multireference treatment should be used. The MRCI-F12+Q computations account for the system's multireference nature but lack size-consistency, a limitation only partially mitigated by the Davidson (Q) correction. We therefore also computed this PES using the CCSDT(Q) method, which extends coupled-cluster theory to include full triples excitations (CCSDT) with a perturbative treatment of connected quadruple excitations. However, both the MRCI-F12+Q and CCSDT(Q) methods significantly under-predicted the $E0$ values of nearly all wells relative to the ATcT data (Tables 1 and 2). The CCSD(T)-F12a level, on the other hand, produced highly accurate zero-point energy predictions when compared to ATcT values (Tables 1 and 2).

The CCSD(T)-F12a/aug-cc-pVTZ-F12 energies computed here are in excellent agreement with the complete basis set extrapolation value based on CCSD(T) energies reported in the literature (Fig. 5). The MRCI calculations, both with and without the explicit F12 correlation[75] or the Davidson correction,[76] consistently produced lower energies than the CCSD(T) values (Fig. 5). Similarly, MRCI-F12+Q yielded lower energies than the ATcT values (Tables 1 and 2). The inclusion of the F12 correlation reduced the CCSD(T) energies but increased the MRCI energies. Since the CCSD(T)-F12a/aug-cc-pVTZ-F12 energies showed excellent agreement with both the literature CCSD(T)/CBS values (Fig. 5) and the ATcT values for the wells (Table 2), they were used in this work to compute rate coefficients. The computed pressure-dependent reaction rate coefficients are reported in Tables S4 and S5 (ESI†).

The primary products of NH_2 + NH(T) association at all relevant pressures (1–100 bar) are N_2H_2 + H, primarily the *trans* N_2H_2 isomer due to the lower energy barrier for its formation (Fig. 2 and 6). At high pressures, N_2H_3 formation becomes relevant but only plays a significant role at temperatures below 1000 K (Fig. 6). The pressure dependence of NH_2 + NH(T) reactions was found to be significant only for the isomer products, N_2H_3 and NH_3N; the rate coefficients of bimolecular products that result from well-skipping reactions showed negligible pressure effect (not shown). As expected, the isomers reach thermal equilibrium more rapidly at higher pressures.

The association of $H_2NN(S)$ + H exhibits more complex pressure-dependent branching (Fig. 7) than the NH_2 + NH(T)

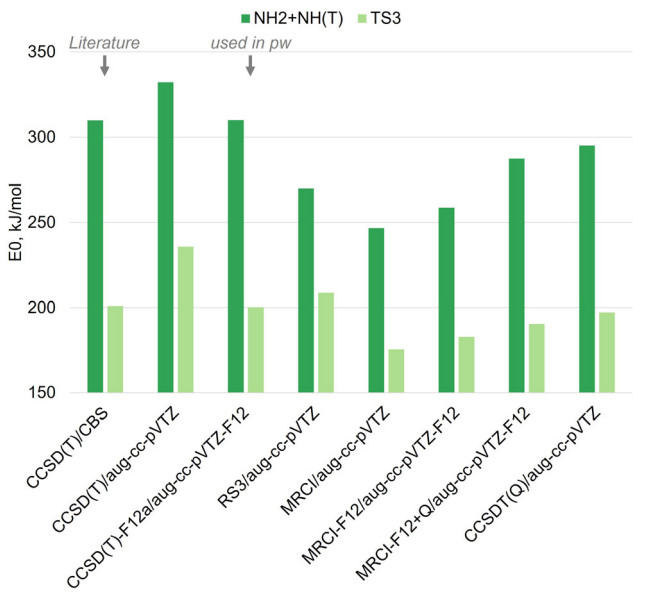

Fig. 5 Zero-point energy comparisons of the NH_2 + NH(T) well and of TS3, both relative to the zero-point energy of the N_2H_3 isomer at the respective level. The CCSD(T)/CBS values were taken from Klippenstein *et al.*[52] (annotated as "Literature" in the figure). All other data were computed in the present work, and the CCSD(T)-F12a/aug-cc-pVTZ-F12 level of theory was further used for kinetic computations in the present work (annotated as "used in pw" in the figure).

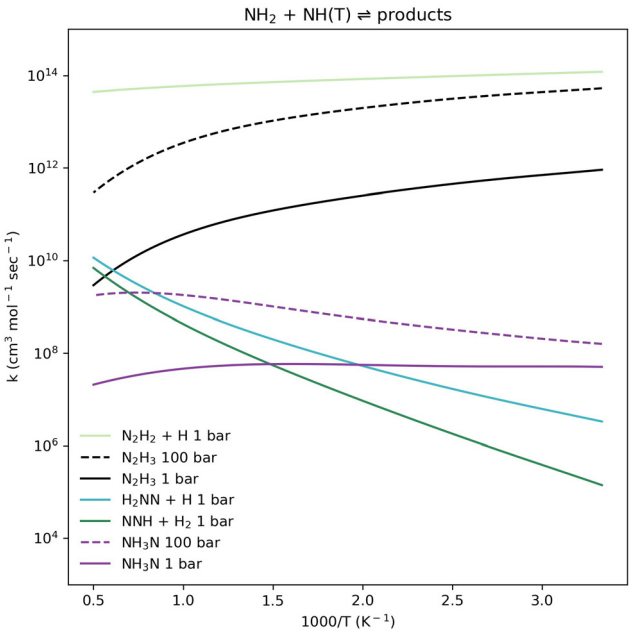

Fig. 6 Comparison of computed rate coefficients for unimolecular NH_2 + NH(T) reactions at 1 and 100 bar. Rate coefficients that do not exhibit a significant pressure-dependence in the examined range are only plotted at 1 bar. The N_2H_2 + H product channel shown here accounts for both *trans* and *cis* N_2H_2 isomers.

channel (Fig. 6), and has not been examined in prior studies of this PES. Similarly to the NH_2 + NH(T) case, the N_2H_2 + H products dominate across almost all relevant temperature and pressure ranges (Fig. 7). The formation of NH_3N becomes the dominant pathway only at relatively low temperatures and high pressures; however, it remains significant across the entire examined temperature range at high pressures. At high temperatures, NNH + H_2 formation becomes important, and NH_2 + NH(T) formation is also a significant minor channel. Vibrationally excited NH_3N species produced by $H_2NN(S)$ + H collisions *via* TS5 are formed well above the TS1 barrier and near or exceeding the TS4 barrier. From the $H_2NN(S)$ + H association direction, once the reactive complex crosses TS5, it can proceed at low pressures past TSs 1, 2, and 3, all of which are submerged relative to TS5. Lower-energy collisions of $H_2NN(S)$ + H can also lead to reactivity *via* a barrierless pathway (Fig. 2), forming N_2H_3 at high pressures. Since NNH + H_2 formation requires a concerted motion of two H atoms (TS4, Fig. 4), it becomes competitive only at high temperatures, while the dominant pathway consists of consecutive single H atom motions, *e.g.*, *via* TS1. At all examined pressures, the significance of NNH + H_2 formation increases with temperature. Consequently, in addition to $H_2NN(S)$ + H ⇌ N_2H_2 + H, the well-skipping $H_2NN(S)$ + H ⇌ NNH + H_2 reaction should be considered in kinetic models of nitrogen-based fuels that describe high-temperature reactivity.

The N_2H_2 + H products are the dominant pathway for NH_2 + NH(T) association at all relevant temperature and pressure ranges (Fig. 6). Our calculated pressure-dependent rate coefficient for the NH_2 + NH(T) ⇌ N_2H_2 + H reaction is benchmarked in Fig. 8. All rate coefficients compared in Fig. 8 show good agreement. The calculated rate coefficients for the

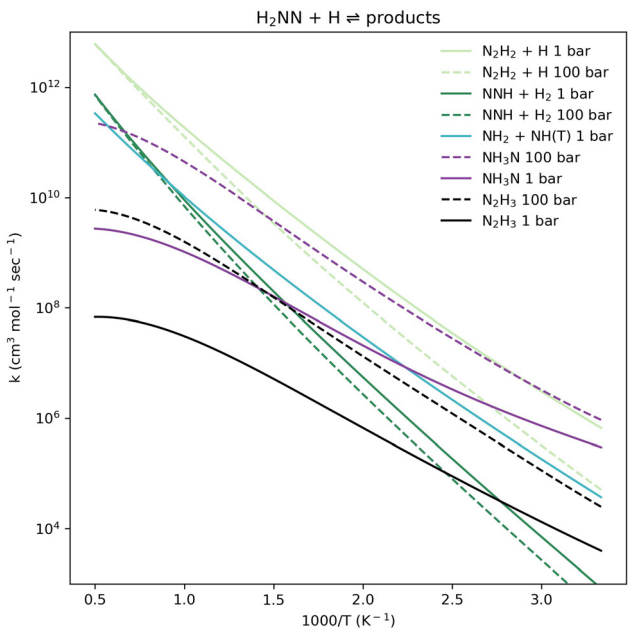

Fig. 7 Comparison of computed rate coefficients for unimolecular $H_2NN(S)$ + H reactions at 1 and 100 bar. Rate coefficients that do not exhibit a significant pressure-dependence in the examined range are only plotted at 1 bar. The N_2H_2 + H product channel shown here accounts for both *trans* and *cis* N_2H_2 isomers.

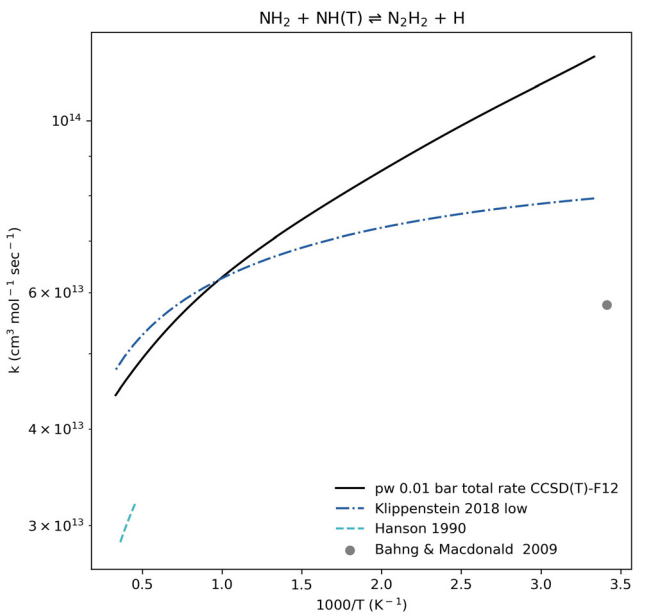

Fig. 8 Rate coefficient comparison for the well-skipping reaction NH_2 + NH(T) ⇌ N_2H_2 + H. The present work (pw) computation shown here accounts for both *trans* and *cis* N_2H_2 isomers at 0.01 bar. The computed rate coefficient is benchmarked against the zero-pressure rate coefficient computed by Kippenstein *et al.*,[52] a rate coefficient determined by Hanson *et al.*[96] based on experimental data at 2200–2800 K and 0.8–1.1 bar, and an experimental result by Bahng and Macdonald[97] at 293 K and pressures up to 0.013 bar.

trans-N_2H_2 product (by Kippenstein *et al.*) or the combined *trans* and *cis* products (reported in the experimental references) are in excellent agreement with values computed in this work, all within a factor of 1.5×. This strong agreement between the computed rate coefficient and experimental data is seen across both low- and high-temperature regions when validated against different sources (Fig. 6).

The rate coefficient of the $NH_2 + NH(T) \rightleftharpoons N_2H_3$ reaction is in the fall-off regime in the mid- and high-temperature range, even at 100 bar (Fig. 9(A)). Our computed high-pressure limit rate coefficient aligns with the Klippenstein *et al.*[52] high-pressure limit rate coefficient (not shown), since it was directly derived from it *via* an ILT. The pressure-dependent rate coefficient computed here shows good agreement with the previously computed high-pressure limit rate coefficient. The low temperature and low pressure rate coefficient reported by Pagsberg and Eriksen[98] in 1979 (Fig. 9(A)) is based on an outdated kinetic model manually fitted to low-pressure measurements. It is therefore unreliable, and the experimental result that was interpreted using this model cannot be given a significant weight in this analysis.

The rate coefficient computed by Diévart and Catoire[53] and reported by them in the reverse direction relative to Klippenstein *et al.*'s high-pressure limit rate coefficient exhibits a different slope compared to the values reported here and compared to the reversed high-pressure limit rate coefficient. At both 1 and 100 bar the Diévart and Catoire rate coefficient is several orders of magnitude lower than the reversed high-pressure limit rate coefficient in most of the explored temperature range (Fig. 9(B)).

The pressure-dependent rate coefficient computed for the $N_2H_3 \rightleftharpoons NH_2 + NH(T)$ reaction is highly sensitive to the energy of TS2 and TS3 relative to the N_2H_3 well (Fig. 10). These transition state barriers dictate the primary competing pathways for N_2H_2 + H formation (Fig. 2), making their accurate determination critical for reliable rate predictions. Additionally, the rate coefficient is sensitive to the energy difference between the N_2H_3 isomer and the $NH_2 + NH(T)$ well (Fig. 10), as this difference influences the overall reaction kinetics. Uncertainties in these energy values were propagated to estimate their impact on the high-pressure limit rate coefficients, as shown in Fig. S10 (ESI†). As shown above, the system's energy strongly depends on the level of theory used (Fig. 5 and Table 1).

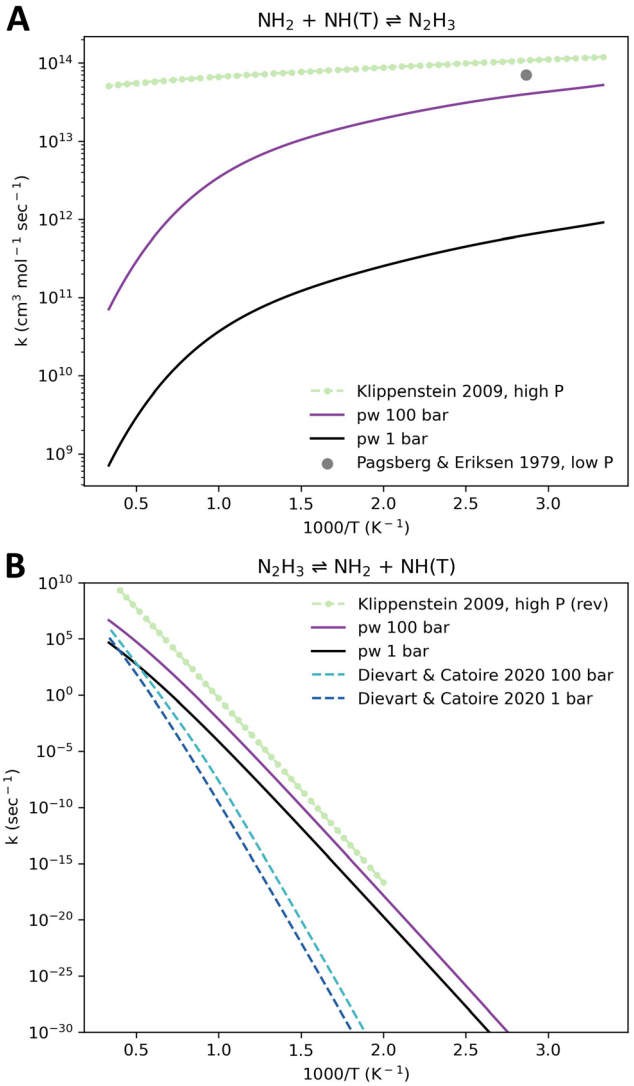

Fig. 9 Rate coefficient comparison for the reaction $NH_2 + NH(T) \rightleftharpoons N_2H_3$ (A) in the forward direction and (B) in the reverse direction. The high-pressure limit rate coefficient computed by Klippenstein *et al.*[52] at CCSD(T)/CBS//CCSD(T)/aug-cc-pVDZ is given in (A) in the original reported direction and in (B) in the reverse direction after being reversed here using thermodynamic data computed by Grinberg Dana *et al.*[8] This rate coefficient was also inferred by Pagsberg and Eriksen[98] at 349 K and a sub-atmospheric pressure on the basis of indirect measurements combined with their model. Diévart and Catoire[53] computed a pressure-dependent rate coefficient in the reverse direction at CCSD(T)/CBS//M062x-D3/aug-cc-pVTZ.

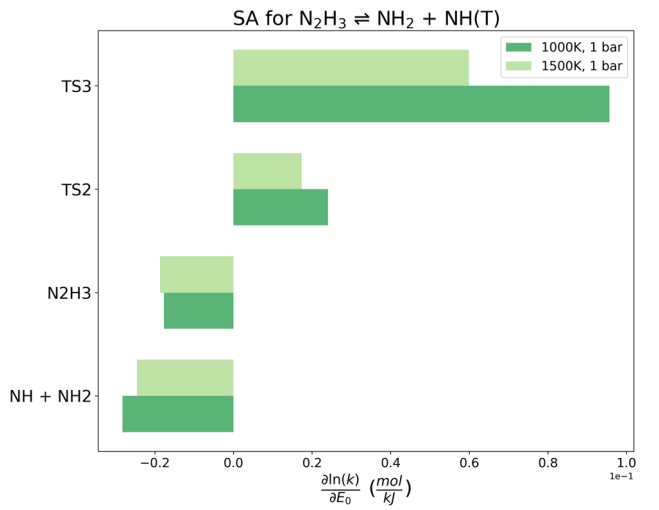

Fig. 10 Normalized sensitivity coefficients of the computed $N_2H_3 \rightleftharpoons NH_2 + NH(T)$ rate coefficient evaluated with respect to the $E0$ values of all wells (the two isomers and bimolecular channels) as well as all TSs on the N_2H_3 PES at 1000 and 1500 K, both at 1 bar. Only the highest normalized sensitivity coefficients are reported.

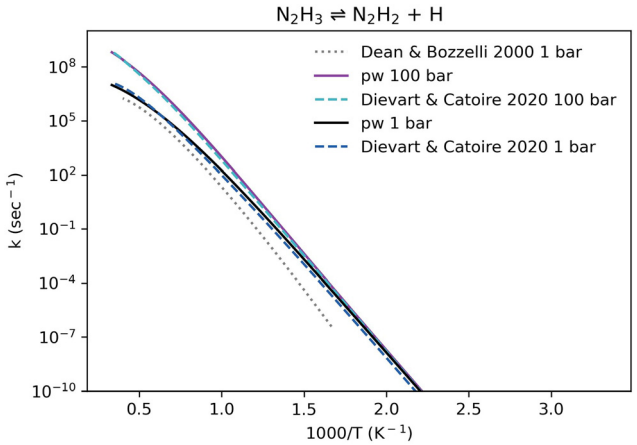

Fig. 11 Rate coefficient comparison for the $N_2H_3 \rightleftharpoons N_2H_2 + H$ reaction. Calculations done in the present work (pw) are shown in this figure as an overall rate coefficient for the formation of both the *trans*-N_2H_2 and the *cis*-N_2H_2 isomers at 1 and 100 bar. The Dean and Bozzelli[88] rate coefficient is given here only at 1 bar (Dean and Bozzelli also reported 0.1 bar and 10 bar values), and the Diévart and Catoire[53] rate coefficient is plotted at both 1 and 100 bar.

The rate coefficient for the $N_2H_3 \rightleftharpoons N_2H_2 + H$ reaction reported by Dean and Bozzelli[88] is lower than that computed in this work at the same pressure (Fig. 11), since Dean and Bozzelli used a significantly higher barrier for this beta-scission reaction. Dean and Bozzelli reported an endothermicity of 226 kJ mol^{-1} for this reaction. The reaction barrier they used is estimated by us to be at least ~238 kJ mol^{-1} based on the reverse energy barrier found here (Fig. 2). This barrier is significantly higher than the *E*0 barrier of 200.6 kJ mol^{-1} computed here for the *trans*-N_2H_2 isomer (Fig. 2). The rate coefficients calculated in the present work and by Diévart and Catoire[53] agree reasonably well (Fig. 11).

4. Conclusions

This study provides a deeper understanding of the N_2H_3 potential energy surface (PES), building upon prior work at the CCSD(T)/CBS level. This work identified the NH_3N isomer as an important well in the N_2H_3 PES, which introduces three new bimolecular wells: NNH + H_2, H_2NN + H, and NH_3 + N(D). The $N_2H_3 \rightleftharpoons NH_2$ + NH(T) rate coefficient was improved compared to previous calculations, and the computed NH_2 + NH(T) $\rightleftharpoons$ N_2H_2 + H rate coefficient shows strong agreement with experimental measurements across both high and low temperatures. The NH_2 + NH(T) reaction predominantly yields N_2H_2 + H on the doublet surface, with N_2H_3 formation becoming significant at low temperatures and high pressures. For $H_2NN(S)$ + H reactions, N_2H_2 + H remains the primary product, with minor contributions from NNH + H_2 and NH_2 + NH(T) at high temperatures; NH_3N formation becomes significant at elevated pressures.

The comprehensive dataset of pressure-dependent rate coefficients presented in this study is valuable for refining models of nitrogen-based fuel combustion and pyrolysis, particularly for ammonia and hydrazine.

Data availability

The data supporting this article have been included as part of the ESI.†

Conflicts of interest

The authors declare that there are no conflicts of interest to disclose.

Acknowledgements

Financial support from the Stephen and Nancy Grand Technion Energy Program (GTEP) is gratefully acknowledged.

References

1 O. Elishav, B. Mosevitzky Lis, E. M. Miller, D. J. Arent, A. Valera-Medina and A. Grinberg Dana, *et al.*, Progress and Prospective of Nitrogen-Based Alternative Fuels, *Chem. Rev.*, 2020, **120**(12), 5352–5436.
2 G. P. Sutton and O. Biblarz, *Rocket Propulsion Elements*, Wiley, 9th edn, 2019.
3 E. F. Rothgery, *Hydrazine and Its Derivatives*, John Wiley & Sons, Ltd, 2004.
4 A. Grinberg Dana, G. E. Shter and G. S. Grader, Nitrogen-based alternative fuel: an environmentally friendly combustion approach, *RSC Adv.*, 2014, **4**, 10051–10059, DOI: 10.1039/C3RA47890D.
5 A. Grinberg Dana, G. E. Shter and G. S. Grader, Nitrogen-Based Alternative Fuels: Progress and Future Prospects, *Energy Technol.*, 2016, **4**(1), 7–18, DOI: 10.1002/ente.201500232.
6 O. Herbinet, P. Bartocci and A. Grinberg Dana, On the use of ammonia as a fuel – A perspective, *Fuel Commun.*, 2022, **11**, 100064.
7 A. Grinberg Dana, O. Elishav, A. Bardow, G. E. Ster and G. S. Grader, Nitrogen-Based Fuels: A Power-to-Fuel-to-Power Analysis, *Angew. Chem., Int. Ed.*, 2016, **55**(31), 8798–8805.
8 A. Grinberg Dana, K. Kaplan, M. Keslin, C. Cao and W. H. Green, Thermodynamic and Chemical Kinetic Parameters in Ammonia Oxidation: A Comparison of Recent Studies and Parameter Recommendations, *Energy Fuels*, 2024, **38**(22), 22482–22500.
9 P. Gray, J. C. Lee and M. Spencer, Combustion, flame and explosion of hydrazine and ammonia I—The spontaneous ignition of pure gaseous hydrazine, *Combust. Flame*, 1963, **7**, 315–321. Available from: https://www.sciencedirect.com/science/article/pii/0010218063902062.
10 M. Auzanneau and M. Roux, Self-Detonation Range in Inert Atmosphere of Ternary Systems Using Hydrogen Peroxide and Hydrazine or Hydrazine Derivatives, *Combust. Sci. Technol.*, 1990, **73**(4–6), 505–520.
11 J. C. Leyer, A. A. Borisov, A. L. Kuhl and W. A. Sirignano, *Dynamics of Detonations and Explosions: Detonations*, American Institute of Aeronautics and Astronautics, Washington DC, 1991, DOI: 10.2514/4.866067.

12 M. Rath, H. Schmitz and M. Steenborg In: Development of a 400 N hydrazine thruster for ESA's Atmospheric Reentry Demonstrator; 1996. Available from: DOI: 10.2514/6.1996-2866.
13 A. S. Yang and T. C. Kuo, Design Analysis of a Satellite Hydrazine Propulsion System, *J. Propul. Power*, 2002, **18**(2), 270–279.
14 K. Anflo, R. Mollerberg, K. Neff and P. King In: High Performance Green Propellant for Satellite Applications. Aerospace Research Central; 2009. Available from: DOI: 10.2514/6.2009-4878.
15 A. M. Elbaz, S. Wang, T. F. Guiberti and W. L. Roberts, Review on the recent advances on ammonia combustion from the fundamentals to the applications, *Fuel Commun.*, 2022, **10**, 100053. Available from: https://www.sciencedirect.com/science/article/pii/S266605202200005X.
16 P. V. Blarigan Advanced internal combustion engine research. DOE Hydrogen Program Review NREL-CP-570-28890. 2000:1-19.
17 C. H. Christensen, T. Johannessen, R. Z. Sørensen and J. K. Nørskov, Towards an ammonia-mediated hydrogen economy?, *Catal. Today*, 2006, **111**(1), 140–144. Frontiers in Catalysis: A Molecular View of Industrial Catalysis. Available from: https://www.sciencedirect.com/science/article/pii/S0920586105007157.
18 P. J. Feibelman and R. Stumpf Comments on potential roles of ammonia in a hydrogen economy—a study of issues related to the use of ammonia for on-board vehicular hydrogen storage; 2006. https://www.pc.gov.au/inquiries/completed/climate-change-adaptation/submissions/sub046-attachment7.pdf.
19 P. Glarborg, J. A. Miller, B. Ruscic and S. J. Klippenstein, Modeling nitrogen chemistry in combustion, *Prog. Energy Combust. Sci.*, 2018, **67**, 31–68.
20 K. P. Shrestha, L. Seidel, T. Zeuch and F. Mauss, Detailed Kinetic Mechanism for the Oxidation of Ammonia Including the Formation and Reduction of Nitrogen Oxides, *Energy Fuels*, 2018, **32**(10), 10202–10217.
21 B. Mei, X. Zhang, S. Ma, M. Cui, H. Guo and Z. Cao, *et al.*, Experimental and kinetic modeling investigation on the laminar flame propagation of ammonia under oxygen enrichment and elevated pressure conditions, *Combust. Flame*, 2019, **210**, 236–246. Available from: https://www.sciencedirect.com/science/article/pii/S0010218019303979.
22 A. Stagni, C. Cavallotti, S. Arunthanayothin, Y. Song, O. Herbinet and F. Battin-Leclerc, *et al.*, An experimental, theoretical and kinetic-modeling study of the gas-phase oxidation of ammonia, *React. Chem. Eng.*, 2020, **5**, 696–711, DOI: 10.1039/C9RE00429G.
23 S. Arunthanayothin, A. Stagni, Y. Song, O. Herbinet, T. Faravelli and F. Battin-Leclerc, Ammonia-methane interaction in jet-stirred and flow reactors: An experimental and kinetic modeling study, *Proc. Combust. Inst.*, 2021, **38**(1), 345–353. Available from: https://www.sciencedirect.com/science/article/pii/S1540748920304934.
24 A. Bertolino, M. Fürst, A. Stagni, A. Frassoldati, M. Pelucchi and C. Cavallotti, *et al.*, An evolutionary, data-driven approach for mechanism optimization: theory and application to ammonia combustion, *Combust. Flame*, 2021, **229**, 111366. Available from: https://www.sciencedirect.com/science/article/pii/S0010218021000754.
25 K. P. Shrestha, C. Lhuillier, A. A. Barbosa, P. Brequigny, F. Contino and C. Mounaïm-Rousselle, *et al.*, An experimental and modeling study of ammonia with enriched oxygen content and ammonia/hydrogen laminar flame speed at elevated pressure and temperature, *Proc. Combust. Inst.*, 2021, **38**(2), 2163–2174. Available from: https://www.sciencedirect.com/science/article/pii/S1540748920302881.
26 K. P. Shrestha, B. R. Giri, A. M. Elbaz, G. Issayev, W. L. Roberts and L. Seidel, *et al.*, A detailed chemical insights into the kinetics of diethyl ether enhancing ammonia combustion and the importance of NOx recycling mechanism, *Fuel Commun.*, 2022, **10**, 100051. Available from: https://www.sciencedirect.com/science/article/pii/S2666052022000036.
27 J. Zhang, B. Mei, W. Li, J. Fang, Y. Zhang and C. Cao, *et al.*, Unraveling Pressure Effects in Laminar Flame Propagation of Ammonia: A Comparative Study with Hydrogen, Methane, and Ammonia/Hydrogen, *Energy Fuels*, 2022, **36**(15), 8528–8537.
28 J. Liu, C. Zou and J. Luo, Experimental and modeling study on the ignition delay times of ammonia/methane mixtures at high dilution and high temperatures, *Proc. Combust. Inst.*, 2022, 4399–4407. Available from: https://www.sciencedirect.com/science/article/pii/S1540748922005284.
29 R. Tang, Q. Xu, J. Pan, J. Gao, Z. Wang and H. Wei, *et al.*, An experimental and modeling study of ammonia oxidation in a jet stirred reactor, *Combust. Flame*, 2022, **240**, 112007. Available from: https://www.sciencedirect.com/science/article/pii/S0010218022000268.
30 P. García-Ruiz, M. Uruén, M. Abián and M. U. Alzueta, High pressure ammonia oxidation in a flow reactor, *Fuel*, 2023, **348**, 128302 Available from: https://www.sciencedirect.com/science/article/pii/S0016236123009158.
31 X. Zhang, K. K. Yalamanchi and S. Mani Sarathy, Combustion chemistry of ammonia/C1 fuels: A comprehensive kinetic modeling study, *Fuel*, 2023, **341**, 127676. Available from: https://www.sciencedirect.com/science/article/pii/S0016236123002892.
32 Y. Zhu, H. J. Curran, S. Girhe, Y. Murakami, H. Pitsch and K. Senecal, *et al.*, The combustion chemistry of ammonia and ammonia/hydrogen mixtures: A comprehensive chemical kinetic modeling study, *Combust. Flame*, 2024, **260**, 113239. Available from: https://www.sciencedirect.com/science/article/pii/S0010218023006132.
33 A. S. Singh, S. Mohapatra, R. Boyapati, A. M. Elbaz, S. K. Dash and W. L. Roberts, *et al.*, Chemical Kinetic Modeling of the Autoignition Properties of Ammonia at Low-Intermediate Temperature and High Pressure using a Newly Proposed Reaction Mechanism, *Energy Fuels*, 2021, **35**(16), 13506–13522.
34 M. Hamdy, S. Nadiri, A. Mohamed, S. Dong, Y. Wu and R. Fernandes, *et al.* An Updated Comprehensive Chemical Kinetic Mechanism for Ammonia and its Blends with Hydrogen, Methanol, and N-Heptane. In: WCX SAE World

Congress Experience. SAE International; 2023. Available from: DOI: 10.4271/2023-01-0204.
35 S. Nadiri, B. Shu, C. F. Goldsmith and R. Fernandes, Development of comprehensive kinetic models of ammonia/methanol ignition using Reaction Mechanism Generator (RMG), *Combust. Flame*, 2023, **251**, 112710.
36 J. Bugler, K. P. Somers, J. M. Simmie, F. Güthe and H. J. Curran, Modeling Nitrogen Species as Pollutants: Thermochemical Influences, *J. Phys. Chem. A*, 2016, **120**(36), 7192–7197.
37 S. J. Klippenstein and P. Glarborg, Theoretical kinetics predictions for NH_2 + HO_2, *Combust. Flame*, 2022, **236**, 111787. Available from: https://www.sciencedirect.com/science/article/pii/S0010218021005307.
38 L. Kawka, G. Juhász, M. Papp, T. Nagy, I. G. Zsély and T. Turányi, Comparison of detailed reaction mechanisms for homogeneous ammonia combustion, *Z. Phys. Chem.*, 2020, **234**(7–9), 1329–1357, DOI: 10.1515/zpch-2020-1649.
39 A. Valera-Medina, F. Amer-Hatem, A. K. Azad, I. C. Dedoussi, M. de Joannon and R. X. Fernandes, *et al.*, Review on Ammonia as a Potential Fuel: From Synthesis to Economics, *Energy Fuels*, 2021, **35**(9), 6964–7029.
40 A. A. Konnov and J. De Ruyck, Kinetic modeling of the decomposition and flames of hydrazine, *Combust. Flame*, 2001, **124**(1), 106–126. Available from: https://www.sciencedirect.com/science/article/pii/S0010218000001875.
41 Y. Ichiro Izato, K. Shiota and A. Miyake, A detailed mechanism for the initial hypergolic reaction in liquid hydrazine/nitrogen tetroxide mixtures based on quantum chemistry calculations, *Combust. Flame*, 2021, **229**, 111389. Available from: https://www.sciencedirect.com/science/article/pii/S0010218021001048.
42 R. Asatryan, J. W. Bozzelli, G. D. Silva, S. Swinnen and M. T. Nguyen, Formation and Decomposition of Chemically Activated and Stabilized Hydrazine, *J. Phys. Chem. A*, 2010, **114**(21), 6235–6249.
43 P. Raghunath, N. T. Nghia and M. C. Lin, Chapter Seven – *Ab Initio* Chemical Kinetics of Key Processes in the Hypergolic Ignition of Hydrazine and Nitrogen Tetroxide, in *Energetic Materials*, ed. J. R. Sabin, Academic Press, 2014, vol. 69 of Advances in Quantum Chemistry, pp. 253–301. Available from: https://www.sciencedirect.com/science/article/pii/B9780128003459000076.
44 Y. Daimon, H. Terashima and M. Koshi, Chemical Kinetics of Hypergolic Ignition in Hydrazine/Nitrogen-dioxide Gas Mixtures, Available from: DOI: 10.2514/6.2013-159.
45 L. Zhang, A. C. Tv Duin, S. V. Zybin and W. A. Goddard III, Thermal Decomposition of Hydrazines from Reactive Dynamics Using the ReaxFF Reactive Force Field, *J. Phys. Chem. B*, 2009, **113**(31), 10770–10778.
46 M. W. Schmidt and M. S. Gordon, The Decomposition of Hydrazine in the Gas Phase and over an Iridium Catalyst, *Z. Phys. Chem.*, 2013, **227**(11), 1301–1336, DOI: 10.1524/zpch.2013.0404.
47 S. S. Tafreshi, A. Roldan and N. H. de Leeuw, Density functional theory calculations of the hydrazine decomposition mechanism on the planar and stepped Cu(111) surfaces, *Phys. Chem. Chem. Phys.*, 2015, **17**, 21533–21546, DOI: 10.1039/C5CP03204K.
48 H. Sun and C. K. Law, Thermochemical and Kinetic Analysis of the Thermal Decomposition of Monomethylhydrazine: An Elementary Reaction Mechanism, *J. Phys. Chem. A*, 2007, **111**(19), 3748–3760.
49 P. Zhang, S. J. Klippenstein, H. Sun and C. K. Law, *Ab initio* kinetics for the decomposition of monomethylhydrazine (CH3NHNH2), *Proc. Combust. Inst.*, 2011, **33**(1), 425–432. Available from: https://www.sciencedirect.com/science/article/pii/S1540748910000350.
50 P. Zhang, S. J. Klippenstein, L. B. Harding, H. Sun and C. K. Law, Secondary channels in the thermal decomposition of monomethylhydrazine (CH_3NHNH_2), *RSC Adv.*, 2014, **4**, 62951–62964, DOI: 10.1039/C4RA13131B.
51 J. Wu, F. N. O. Bruce, X. Bai, X. Ren and Y. Li, Insights into the Reaction Kinetics of Hydrazine-Based Fuels: A Comprehensive Review of Theoretical and Experimental Methods, *Energies*, 2023, **16**(16), 6006. Available from: https://www.mdpi.com/1996-1073/16/16/6006.
52 S. J. Klippenstein, L. B. Harding, B. Ruscic, R. Sivaramakrishnan, N. K. Srinivasan and M. C. Su, *et al.*, Thermal Decomposition of NH2OH and Subsequent Reactions: *Ab Initio* Transition State Theory and Reflected Shock Tube Experiments, *J. Phys. Chem. A*, 2009, **113**(38), 10241–10259.
53 P. Diévart and L. Catoire, Contributions of Experimental Data Obtained in Concentrated Mixtures to Kinetic Studies: Application to Monomethylhydrazine Pyrolysis, *J. Phys. Chem. A*, 2020, **124**(30), 6214–6236.
54 P. K. Venkatesh, R. W. Carr, M. H. Cohen and A. M. Dean, Microcanonical Transition State Theory Rate Coefficients from Thermal Rate Constants *via* Inverse Laplace Transformation, *J. Phys. Chem. A*, 1998, **102**, 8104–8115.
55 A. Grinberg Dana, D. Ranasinghe, H. Wu, C. Grambow, X. Dong and M. Johnson, *et al.*, *ARC – Automated Rate Calculator, version 1.1.0.*, GitHub, 2019, https://github.com/ReactionMechanismGenerator/ARC.
56 G. Landrum RDKit: Open-Source Cheminformatics Software;. https://www.rdkit.org. Available from: https://www.rdkit.org.
57 T. A. Halgren, MMFF VI. MMFF94s option for energy minimization studies, *J. Comput. Chem.*, 1999, **20**(7), 720–729.
58 J. D. Chai and M. Head-Gordon, Long-range corrected hybrid density functionals with damped atom-atom dispersion corrections, *Phys. Chem. Chem. Phys.*, 2008, **10**, 6615–6620, DOI: 10.1039/B810189B.
59 F. Weigend and R. Ahlrichs, Balanced basis sets of split valence, triple zeta valence and quadruple zeta valence quality for H to Rn: Design and assessment of accuracy, *Phys. Chem. Chem. Phys.*, 2005, **7**, 3297–3305, DOI: 10.1039/B508541A.
60 S. Grimme, Semiempirical hybrid density functional with perturbative second-order correlation, *J. Chem. Phys.*, 2006, **124**(3), 034108, DOI: 10.1063/1.2148954.
61 S. Grimme, J. Antony, S. Ehrlich and H. Krieg, A consistent and accurate *ab initio* parametrization of density functional

dispersion correction (DFT-D) for the 94 elements H-Pu, *J. Chem. Phys.*, 2010, **132**(15), 154104, DOI: 10.1063/1.3382344.

62 J. Dunning and H. Thom, Gaussian basis sets for use in correlated molecular calculations. I. The atoms boron through neon and hydrogen, *J. Chem. Phys.*, 1989, **90**(2), 1007–1023, DOI: 10.1063/1.456153.

63 I. M. Alecu, J. Zheng, Y. Zhao and D. G. Truhlar, Computational Thermochemistry: Scale Factor Databases and Scale Factors for Vibrational Frequencies Obtained from Electronic Model Chemistries, *J. Chem. Theory Comput.*, 2010, **6**(9), 2872–2887.

64 C. Eckart, The Penetration of a Potential Barrier by Electrons, *Phys. Rev.*, 1930, **35**(11), 1303–1309.

65 K. Fukui, The path of chemical reactions-the IRC approach, *Acc. Chem. Res.*, 1981, **14**(12), 363–368.

66 A. Grinberg Dana, M. Liu and W. H. Green, Automated chemical resonance generation and structure filtration for kinetic modeling, *Int. J. Chem. Kinet.*, 2019, **51**(10), 760–776, DOI: 10.1002/kin.21307.

67 A. Grinberg Dana, M. S. Johnson, J. W. Allen, S. Sharma, S. Raman and M. Liu, *et al.*, Automated reaction kinetics and network exploration (Arkane): A statistical mechanics, thermodynamics, transition state theory, and master equation software, *Int. J. Chem. Kinet.*, 2023, **55**(6), 300–323.

68 M. Liu, A. Grinberg Dana, M. S. Johnson, M. J. Goldman, A. Jocher and A. M. Payne, *et al.*, Reaction Mechanism Generator v3.0: Advances in Automatic Mechanism Generation, *J. Chem. Inf. Model.*, 2021, **61**(6), 2686–2696.

69 M. J. Frisch, G. W. Trucks, H. B. Schlegel, G. E. Scuseria, M. A. Robb and J. R. Cheeseman, *et al.*, *Gaussian 09, Revision D.01*, Gaussian, Inc., Wallingford CT, 2013.

70 T. B. Adler, G. Knizia and H. J. Werner, A simple and efficient CCSD(T)-F12 approximation, *J. Chem. Phys.*, 2007, **127**(22), 221106, DOI: 10.1063/1.2817618.

71 G. Knizia, T. B. Adler and H. J. Werner, Simplified CCSD(T)-F12 methods: Theory and benchmarks, *J. Chem. Phys.*, 2009, **130**(5), 054104.

72 T. B. Adler and H. J. Werner, An explicitly correlated local coupled cluster method for calculations of large molecules close to the basis set limit, *J. Chem. Phys.*, 2011, **135**(14), 144117.

73 K. A. Peterson, T. B. Adler and H. J. Werner, Systematically convergent basis sets for explicitly correlated wavefunctions: The atoms H, He, B–Ne, and Al–Ar, *J. Chem. Phys.*, 2008, **128**(8), 084102, DOI: 10.1063/1.2831537.

74 G. Knizia and H. J. Werner, Explicitly correlated RMP2 for high-spin open-shell reference states, *J. Chem. Phys.*, 2008, **128**(15), 154103.

75 T. Shiozaki and H. J. Werner, Multireference explicitly correlated F12 theories, *Mol. Phys.*, 2013, **111**(5), 607–630.

76 E. R. Davidson and D. W. Silver, Size consistency in the dilute helium gas electronic structure, *Chem. Phys. Lett.*, 1977, **52**(3), 403–406. Available from: https://www.sciencedirect.com/science/article/pii/0009261477804752.

77 S. A. Kucharski and R. J. Bartlett, An efficient way to include connected quadruple contributions into the coupled cluster method, *J. Chem. Phys.*, 1998, **108**(22), 9221–9226.

78 Y. J. Bomble, J. F. Stanton, M. Kállay and J. Gauss, Coupled-cluster methods including noniterative corrections for quadruple excitations, *J. Chem. Phys.*, 2005, **123**(5), 054101.

79 H. J. Werner, P. J. Knowles, G. Knizia, F. R. Manby and M. Schütz, Molpro: a general-purpose quantum chemistry program package, *Wiley Interdiscip. Rev.: Comput. Mol. Sci.*, 2012, **2**(2), 242–253, DOI: 10.1002/wcms.82.

80 D. G. Smith, L. A. Burns, A. C. Simmonett, R. M. Parrish, M. C. Schieber and R. Galvelis, *et al.*, PSI4 1.4: Open-source software for high-throughput quantum chemistry, *J. Chem. Phys.*, 2020, **152**(18), 184108.

81 H. Wu, A. M. Payne, H. W. Pang, A. Menon, C. A. Grambow and D. S. Ranasinghe, *et al.*, Toward Accurate Quantum Mechanical Thermochemistry: (1) Extensible Implementation and Comparison of Bond Additivity Corrections and Isodesmic Reactions, *J. Phys. Chem. A*, 2024, **128**(21), 4335–4352.

82 M. J. Pilling and S. H. Robertson, Master Equation Models for Chemical Reactions of Importance in Combustion, *Annu. Rev. Phys. Chem.*, 2003, **54**, 245–275.

83 A. Y. Chang, J. W. Bozzelli and A. M. Dean, Kinetic Analysis of Complex Chemical Activation and Unimolecular Dissociation Reactions using QRRK Theory and the Modified Strong Collision Approximation, *Z. Phys. Chem.*, 2000, **214**, 1533–1568.

84 J. A. Miller and S. J. Klippenstein, Determining phenomenological rate coefficients from a time-dependent, multiple-well master equation: ''species reduction'' at high temperatures, *Phys. Chem. Chem. Phys.*, 2013, **15**(13), 4744–4753.

85 M. S. Johnson, X. Dong, A. Grinberg Dana, Y. Chung, D. J. Farina and R. J. Gillis, *et al.*, RMG Database for Chemical Property Prediction, *J. Chem. Inf. Model.*, 2022, **62**(20), 4906–4915.

86 A. W. Jasper and J. A. Miller, Lennard-Jones parameters for combustion and chemical kinetics modeling from full-dimensional intermolecular potentials, *Combust. Flame*, 2014, **161**(1), 101–110.

87 P. K. Venkatesh, A. M. Dean, M. H. Cohen and R. W. Carr, Chebyshev expansions and sensitivity analysis for approximating the temperature-and pressure-dependence of chemically-activated reactions, *Rev. Chem. Eng.*, 1997, **13**(1), 1–67.

88 A. M. Dean and J. W. Bozzelli, Combustion chemistry of nitrogen, *Gas-phase combustion chemistry*, Springer, 2000, pp. 125–341.

89 D. Weininger, SMILES, a chemical language and information system. 1. Introduction to methodology and encoding rules, *J. Chem. Inf. Comput. Sci.*, 1988, **28**(1), 31–36.

90 N. Balucani, A. Bergeat, L. Cartechini, G. G. Volpi, P. Casavecchia and D. Skouteris, *et al.*, Combined crossed molecular beam and theoretical studies of the N (2D) + CH_4 reaction and implications for atmospheric models of Titan, *J. Phys. Chem. A*, 2009, **113**(42), 11138–11152.

91 G. Faingold and J. K. Lefkowitz, A numerical investigation of NH_3/O_2/He ignition limits in a non-thermal plasma, *Proc.*

Combust. Inst., 2021, **38**(4), 6661–6669Available from: https://www.sciencedirect.com/science/article/pii/S1540748920306179.

92 B. Ruscic Active Thermochemical Tables (ATcT) values based on ver. 1.130 of the Thermochemical Network, 2024;. https://atct.anl.gov/ (Accessed August 2024).

93 T. J. Lee and P. R. Taylor, A diagnostic for determining the quality of single-reference electron correlation methods, *Int. J. Quantum Chem.*, 1989, **36**(S23), 199–207, DOI: 10.1002/qua.560360824.

94 D. Jayatilaka and T. J. Lee, Open–shell coupled–cluster theory, *J. Chem. Phys.*, 1993, **98**(12), 9734–9747, DOI: 10.1063/1.464352.

95 T. J. Lee and G. E. Scuseria, in *Achieving Chemical Accuracy with Coupled-Cluster Theory*, ed. S. R. Langhoff, Springer, Dordrecht, Netherlands, 1995. pp. 47–108. Available from: DOI: 10.1007/978-94-011-0193-6_2.

96 D. F. Davidson, K. Kohse-Höinghaus, A. Y. Chang and R. K. Hanson, A pyrolysis mechanism for ammonia, *Int. J. Chem. Kinet.*, 1990, **22**(5), 513–535.

97 M. K. Bahng and R. G. Macdonald, Determination of the rate constants for the radical-radical reactions NH2(X2B1) + NH(X3Σ-) and NH2(X2B1) + H(2S) at 293 K, *J. Phys. Chem. A*, 2009, **113**(11), 2415–2423.

98 P. B. Pagsberg, J. Eriksen and H. Christensen, Pulse radiolysis of gaseous ammonia–oxygen mixtures, *J. Phys. Chem.*, 1979, **83**(5), 582–590.